Modelled Rainfall Response to Strong El Niño Sea Surface Temperature Anomalies in the Tropical Pacific

Christine T. Y. Chung and Scott B. Power

Centre for Australian Weather and Climate Research, Bureau of Meteorology, Melbourne, Victoria, Australia

(Manuscript received 2 September 2014, in final form 1 December 2014)

ABSTRACT

El Niño–Southern Oscillation strongly influences the interannual variability of rainfall over the Pacific, shifting the position and orientation of the South Pacific convergence zone (SPCZ) and intertropical convergence zone (ITCZ). In 1982/83 and 1997/98, very strong El Niño events occurred, during which time the SPCZ and ITCZ merged into a single zonal convergence zone (szCZ) extending across the Pacific at approximately 5°S. The sea surface temperature anomalies (SSTAs) reached very large values and peaked farther east compared to other El Niño events. Previous work shows that tropical Pacific precipitation responds nonlinearly to changing the amplitude of the El Niño SSTA even if the structure of the SSTA remains unchanged, but large canonical El Niño SSTAs cannot reproduce the szCZ precipitation pattern. This study conducts idealized, SST-forced experiments, starting with a large-amplitude canonical El Niño SSTA and gradually adding a residual pattern until the full (1982/83) and (1997/98) mean SST is reproduced. Differences between the canonical and strong El Niño SSTA patterns are crucial in generating an szCZ event. Three elements influence the precipitation pattern: (i) the local meridional SST maxima influences the ITCZ position and western Pacific precipitation, (ii) the total zonal SST maximum influences the SPCZ position, and (iii) the equatorial Pacific SST influences the total amount of precipitation. In these experiments, the meridional SST gradient increases as the SSTAs approach szCZ conditions. Additionally, the precipitation changes evident in szCZ years are primarily driven by changes in the atmospheric circulation, rather than thermodynamic changes. The addition of a global warming SST pattern increases the precipitation along the equator and shifts the ITCZ farther equatorward.

1. Introduction

El Niño–Southern Oscillation (ENSO) is the main mode of interannual climate variability over the Pacific (Philander 1990; McPhaden et al. 2006; Australian Bureau of Meteorology and CSIRO 2011a,b). During El Niño (EN) years, rainfall over the South Pacific convergence zone (SPCZ) generally increases and shifts northward. However, in recent years, it has been noted that not all El Niño events generate the same SST anomaly pattern and rainfall response. In the wet seasons (November–April) of 1982/83 and 1997/98, the SPCZ merged with the intertropical convergence zone (ITCZ) into a single zonal convergence zone (szCZ) stretching across the entire Pacific (e.g., Vincent et al. 2011; Cai et al. 2012; Murphy et al. 2014). The panels in Fig. 1 show (Fig. 1a) the observed climatological 1979–2009 November–April rainfall, (Fig. 1b) the rainfall averaged over all EN years, and (Fig. 1c) the rainfall averaged over the two szCZ events. EN years are defined here to be years in which the Southern Oscillation index averaged over the period June–December was less than 5 (Power et al. 2006; Chung et al. 2013). In Fig. 1, we plot the local precipitation maxima (measured north–south) as a simple way to trace the ITCZ and SPCZ. The black lines, showing the climatological precipitation maxima, are plotted in all three panels to highlight the shifts in the ITCZ and SPCZ. From Fig. 1b, the composite EN precipitation maxima (orange lines) show no change in the position of the ITCZ and a slight zonal shift of the SPCZ compared to climatology. The precipitation maxima for

Corresponding author address: Christine Chung, Centre for Australian Weather and Climate Research, Bureau of Meteorology, GPO Box 1289, Melbourne, VIC 3001, Australia.
E-mail: c.chung@bom.gov.au

DOI: 10.1175/JCLI-D-14-00610.1

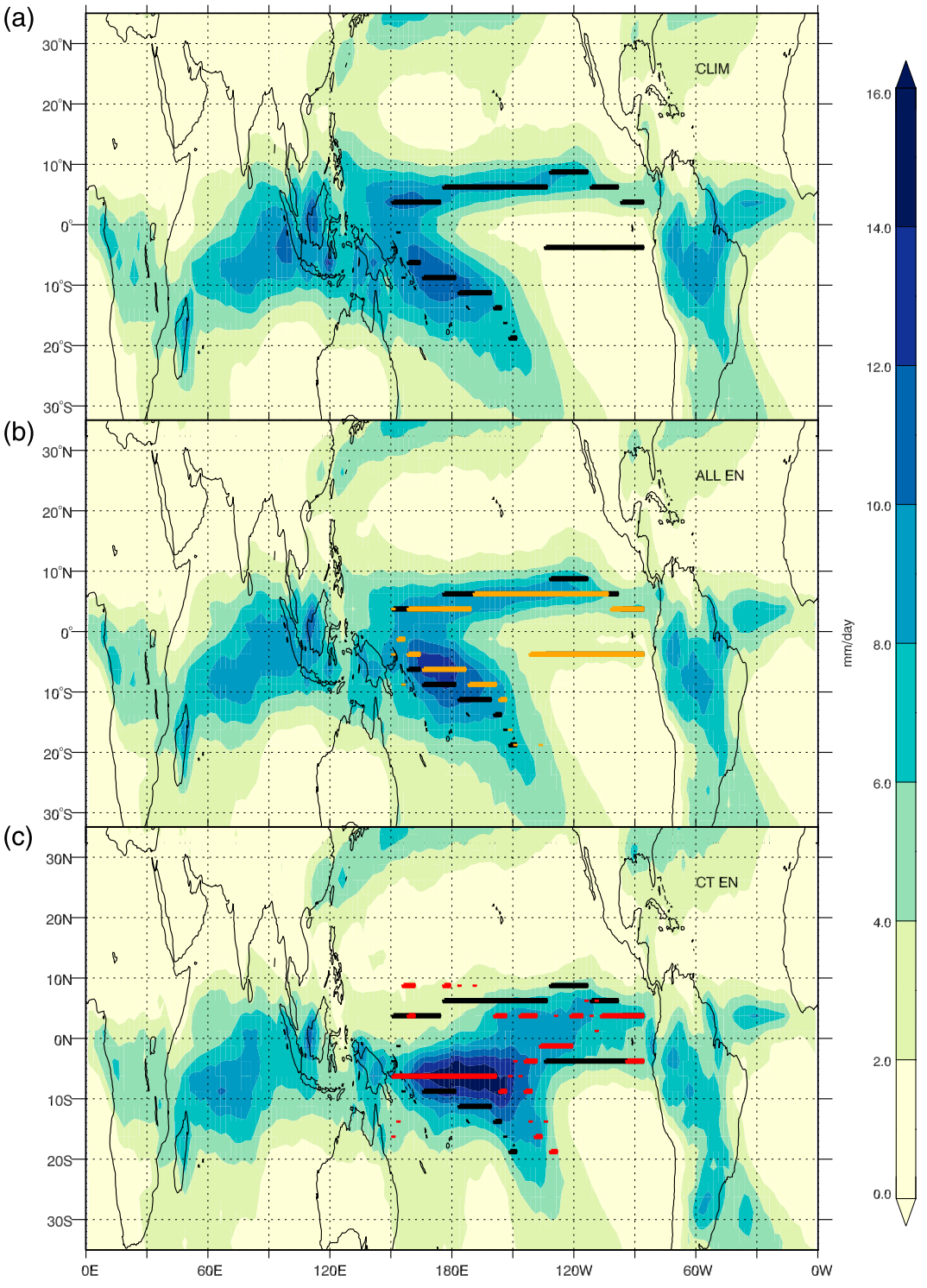

FIG. 1. CMAP observations of November–April rainfall over the tropics. (a) The 1979–2009 climatology, (b) composite of all El Niño years, and (c) composite of CT El Niño years. Local precipitation maxima (measured north–south) are denoted by black lines (for climatology), orange lines (for all El Niño years), and red lines (for CT El Niño years).

cold tongue (CT) EN events (red lines in Fig. 1c) show a significant equatorward shift of the ITCZ and a zonally oriented SPCZ between approximately 150°E and 160°W.

The detailed structure of SST anomalies during EN years has received considerable attention in recent years. For example, EN events have been classified into CT, warm pool (WP), and mixed EN events (Yeh et al. 2009; Kug et al. 2009; Murphy et al. 2014). According to the classification of Kug et al. (2009) and Murphy et al. (2014), CT events feature the largest SST anomalies, with warmer SSTs over the eastern Pacific (5°S–5°N, 150°–90°W) and cooler SSTs over the west. Only two CT events have been observed since 1979, coinciding with the two szCZ events. WP events are characterized by warm SSTs over the Pacific warm pool (5°S–5°N, 160°E–150°W). In both cases, positive rainfall anomalies occur over regions with warm SSTs and vice versa. The warm SSTs in the eastern Pacific during CT EN events are generated by strong warm vertical advection in the east, whereas during WP EN events, horizontal advection dominates (Kug et al. 2009). CT EN events also last unusually long, until boreal spring, whereas other EN events terminate at the end of winter (McPhaden 1999; Takayabu et al. 1999). Studies have shown that CT EN events peak twice: once in boreal winter and again in spring (Vecchi and Harrison 2006; Lengaigne and Vecchi 2009; Kim and Cai 2013).

The occurrence of szCZ events had severe impacts, including droughts in Pacific island countries located in the western Pacific, coral bleaching, and increased frequency of tropical cyclones (Vincent et al. 2011; Cai et al. 2012; Murphy et al. 2014). A study of selected coupled general circulation models from the phases 3 and 5 of CMIP (CMIP3 and CMIP5) databases found that increased greenhouse warming in the twenty-first century leads to a near doubling of the frequency of szCZ events in most of the selected models (Cai et al. 2012). Note that only about half of all the CMIP3 and CMIP5 models available were able to reproduce szCZ events well enough to be considered for the study. Cai et al. (2012) found that about half of the szCZ events produced in these models were associated with strong EN events. This suggests that both a change in the background SST structure (namely, a decrease in the meridional SST gradient), as well as the amplitude of the EN SST anomaly, play a role in triggering such events (Cai et al. 2012, 2014).

There is some uncertainty regarding how ENSO and the SPCZ will change in the twenty-first century (Collins et al. 2010; Brown et al. 2011; Widlansky et al. 2013). However, some robust projections can be made. Brown et al. (2011) analyzed SPCZ changes in CMIP3 models, showing that many models predict a contraction of the eastern edge and an increase in precipitation of the SPCZ. They also found a more zonal orientation of the SPCZ during El Niño years. Widlansky et al. (2013) identified thermodynamic (wet gets wetter) and dynamic (warmest gets wetter) processes as the two opposing mechanisms that drive the SPCZ rainfall response. The authors noted that most CMIP3 and CMIP5 models have inherent SST biases, and once removed it is possible instead for the SPCZ to dry if the tropical SST warms less than 3°C in the twenty-first century. Seager et al. (2010) analyzed precipitation minus evaporation ($P - E$) changes in CMIP3 models and found that ENSO-driven $P - E$ variability is projected to increase. Recently, Power et al. (2013) found that in CMIP3 and CMIP5 models, even when there is uncertainty in projected ENSO-driven SST changes, there is widespread agreement in the projected rainfall changes over the equatorial Pacific.

In a previous study, Chung et al. (2013) performed idealized experiments in which a composite El Niño SST anomaly ($\mathrm{SSTA_{EN}}$) was added to 1979–2009 climatological SSTs. The amplitude of $\mathrm{SSTA_{EN}}$ was multiplied linearly by a factor of $1 \leq \alpha \leq 4$ without varying its spatial structure. Chung et al. (2013) found that the precipitation and atmospheric circulation over the Indo-Pacific region responded nonlinearly. Increasing only the amplitude of $\mathrm{SSTA_{EN}}$ without changing the structure of $\mathrm{SSTA_{EN}}$ (i.e., increasing α only) increased the total rainfall along the equator and caused the ITCZ and SPCZ to shift equatorward. However, none of the resulting precipitation patterns closely resembled the observed pattern seen in the szCZ years; the SPCZ maintained a diagonal component in all the experiments. This suggests that either the model is not able to simulate szCZ events given the corresponding SSTA for these years or that nonlinearity in the response to even a very large value of α does not fully account for szCZs.

In this paper, we first show that the atmospheric general circulation model (AGCM) is capable of capturing szCZ events if forced with the observed SSTA for the szCZ years (i.e., SSTA in 1982/83 and 1997/98). We then show that the AGCM is not able to simulate a szCZ if forced by a generic EN SSTA based on all EN events observed during 1979–2009, even if α is set to the best-fit values for 1982/83 and 1997/98. We then examine the SSTA patterns in the szCZ years and determine the deviation of the SSTA away from the best-fit EN composite (i.e., $\mathrm{SSTA}_R = \mathrm{SSTA} - \alpha_{\mathrm{best-fit}} \times \mathrm{SSTA_{EN}}$). We then determine the precipitation response to the SST patterns with and without $\beta\mathrm{SSTA}_R$ included (using $\beta =$ 0.3, 0.6, 1.0, and 1.3), and we determine whether or not the inclusion of $\beta\mathrm{SSTA}_R$ gives a more accurate zonal precipitation event. The AGCM is then forced with $\beta\mathrm{SSTA}_R$ alone (i.e., with α set to zero) in order to determine if szCZs can be generated by $\beta\mathrm{SSTA}_R$ in the absence of an EN SSTA.

To further understand the precipitation responses in the various experiments, they are decomposed into dynamic, thermodynamic, evaporative, and covariant components. Finally, given the important impacts of szCZ events and the prospect that such events will become more frequent under global warming, we also examine the AGCM response to SSTAs in the presence of late twenty-first-century SST and CO_2 conditions.

This paper is structured as follows: Section 2 describes the AGCM, experimental setup, and the response of the AGCM to 1982/83 and 1997/98 SSTAs. In section 3, we discuss the precipitation response as the SST residual pattern $SSTA_R$ is gradually added to a large-amplitude $SSTA_{EN}$. The precipitation changes due to the further addition of a global warming SST pattern are presented in section 4. Finally, we summarize and discuss our results in section 5.

2. Atmospheric model description and experiments

For these experiments, we use the Australian Community Climate and Earth-System Simulator (ACCESS) AGCM described in Chung et al. (2013) and Bi et al. (2012). The AGCM has a nonhydrostatic dynamical core and is based on a version of the Met Office Unified Model (Staniforth et al. 2003; Davies et al. 2005; Martin et al. 2010). The AGCM was configured to have the HadGEM2 (revision 1.0) climate configuration (Martin et al. 2010, 2011) that incorporates sophisticated parameterizations of unresolved physical processes, including those for the boundary layer, convection, clouds, radiation, aerosols, land surface, gravity wave drag, and hydrological cycle. We use the N96 horizontal resolution, equivalent to 1.25° × 1.875° in latitude and longitude, and 38 vertical levels, with the model top placed at ~39 km.

The ACCESS AGCM is forced with annually repeating monthly-mean climatological SSTs derived from the Hurrell et al. (2008) dataset. We use only SSTs from 1979 to 2009 to coincide with GPCP/CMAP precipitation data (Adler et al. 2003; Huffman et al. 2009). We perform two sets of experiments: the first using twentieth-century CO_2 values (346 ppm) and the second applying twenty-first-century CO_2 values (730 ppm) as well as an additional global warming SST pattern.

The experiments are set up to systematically investigate the SST properties necessary to generate a szCZ event. The first step is to test the models precipitation response to a large-amplitude, composite, El Niño SST anomaly. We then investigate how the spatial structure of the SST anomalies in szCZ years drives the zonal precipitation pattern and how this changes under global warming. This extends the work of Chung et al. (2013) by focusing specifically on 1982/83 and 1997/98 and by estimating the role of the $SSTA_R$ in the response. We therefore compare the differences in the precipitation response with three types of SST anomalies added: (i) a large-amplitude composite El Niño SST anomaly, (ii) the averaged SST anomaly from the szCZ El Niño years (1982/83 and 1997/98), and (iii) a global warming pattern.

The three types of SST anomalies are combined as shown in Fig. 2. In Chung et al. (2013), a composite El Niño SST anomaly $SSTA_{EN}$ comprising all events from 1979 to 2009 was added to the climatological SST in multiples of α, ranging 1–4. Anomalies are calculated by subtracting the climatological monthly mean. The years included in the composite are listed in Table 1. Each experiment is run for 20 yr, using annually repeating, monthly-mean SSTs, and the first 5 yr are discarded.

$SSTA_{EN}$ features strong warming along the eastern equatorial Pacific, with warming extending westward to ~160°E and meridionally 20° north and south of the equator. During the szCZ years, the central equatorial Pacific warms less, and the SSTs along the South American coast warm more. The SST anomalies in the $\alpha = 3$ case ($SSTA_{3EN}$, shown in Fig. 2a) are closest in magnitude to the observed szCZ SST anomalies and are used as our control run. We then subtract the SST anomalies from the szCZ years from $SSTA_{3EN}$ to obtain the residual ($SSTA_R$, shown in Fig. 2c), that is,

$$SSTA_R = SSTA_{zonal} - SSTA_{3EN}, \quad (1)$$

where $SSTA_{zonal}$ is the average of the 1982/83 and 1997/98 SST anomalies with respect to climatology. We add $SSTA_R$ to $SSTA_{3EN}$ in multiples of $\beta = 0$, 0.3, 0.6, 1.0, and 1.3. In this way, the $\beta = 0$ case corresponds to the idealized $\alpha = 3$ case used in Chung et al. (2013), and the $\beta = 1$ case corresponds to the observed $SSTA_{zonal}$ (shown in Fig. 2c).

The SST anomaly pattern during CT EN events, $SSTA_{zonal}$, is unique in the following ways: First, the SST anomalies along the equatorial Pacific generated during CT EN events are larger and lie farther east than during other types of EN events. The meridional SST gradients across the central and eastern Pacific are steeper, and a ''horseshoe'' pattern of cold SST anomalies surrounds the warm anomalies in the western and central Pacific.

Table 2 summarizes the two sets of experiments. In the 20C runs, we apply the average of observed 1958–2008 CO_2 levels (346 ppm), kept constant throughout the runs. In the 21C runs, the CO_2 level is increased to 730 ppm and is also kept constant. Additionally, a global warming SST pattern (ΔSST_{GW}) is added to the SSTs. The term ΔSST_{GW} is taken to be the multimodel ensemble-mean (MMEM) change in SST between periods 1980 and 1999

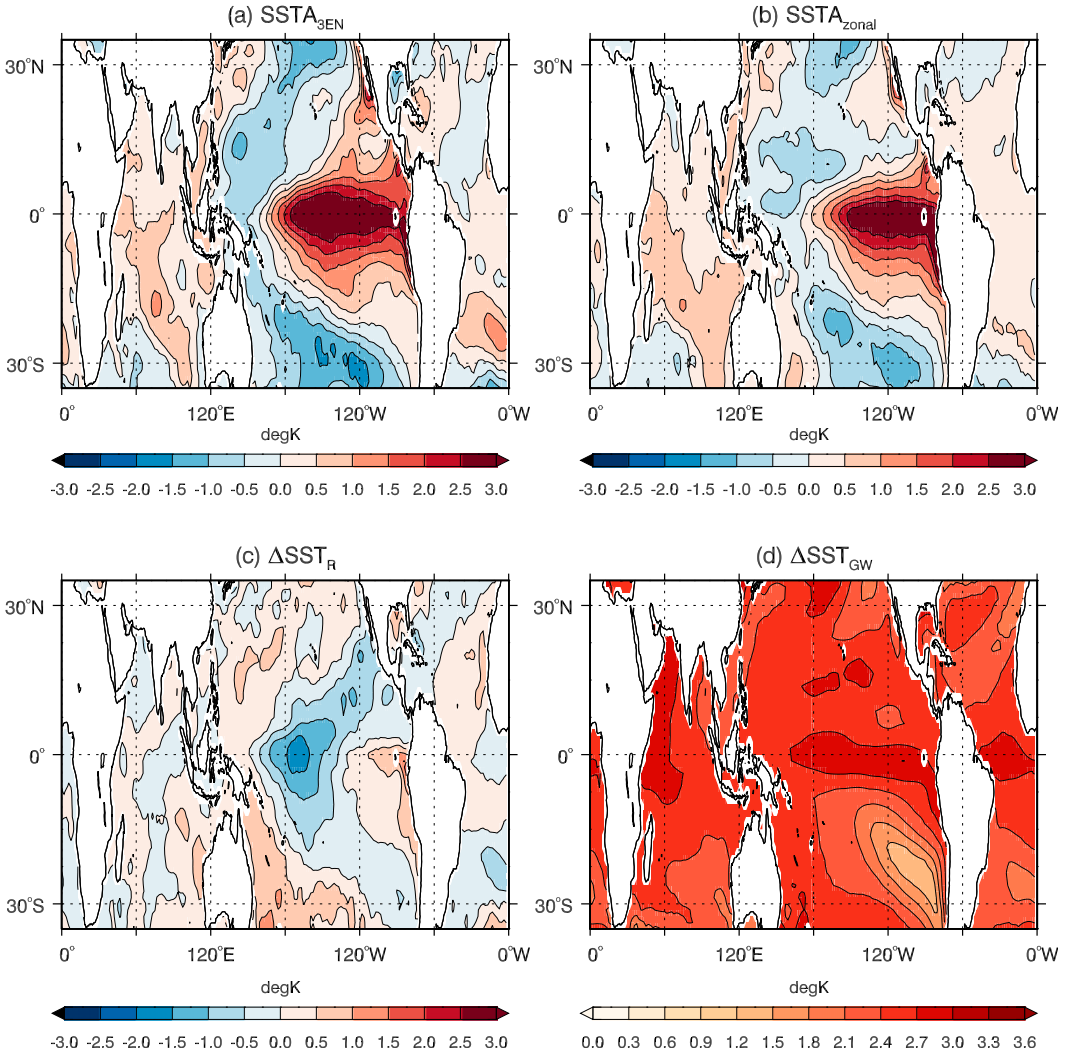

FIG. 2. Types of large EN SST anomalies applied to the 1979–2009 climatological SSTs: (a) 3 times the composite El Niño SST anomaly consisting of all EN events between 1979 and 2009 ($SSTA_{3EN}$); (b) the average of the 1982/83 and 1997/98 SST anomalies ($SSTA_{zonal}$); (c) the residual from (b) minus (a) ($SSTA_R$); and (d) the global warming SST pattern ΔSST_{GW}.

and 2080 and 2099 projected by CMIP3 models under the Special Report on Emissions Scenarios (SRES) A2 scenario (Meehl et al. 2007), shown in Fig. 2d.

Precipitation response to 1982/83 and 1997/98 El Niño SST anomalies

The model's skill in simulating the mean state is discussed in Fig. 1 and section 2 of Chung et al. (2013). The model reproduces the structure and position of the ITCZ and SPCZ well; however, it overestimates the precipitation in these bands by ~5–6 mm day^{-1}.

To test how well the model reproduces szCZ events, we performed an initial experiment in which the model was forced with time-varying SSTs from 1950 to 2011. The 10 ensemble members were generated, using slightly different atmospheric initial conditions for each one. We then compared the November–April mean precipitation response from the model to CMAP observations. Figures 3c and 3d show the model response for 1982/83 and 1997/98, respectively, while Figs. 3e and 3f show the difference between the model response and observations for the same years.

The model generally overestimates the amount of precipitation over the szCZ, especially in the western Pacific. However, the spatial pattern of the szCZ is reasonably well reproduced in both years: the SPCZ and ITCZ are indistinguishable and the variations in the szCZ between the 2 yr are well matched to the observations. The model therefore performs well enough to test our hypotheses.

TABLE 1. List of El Niño years between 1979 and 2009 used to create the composite for the AGCM experiments.

El Niño years 1979–2009
1982
1987
1991
1992
1993
1994
1997
2002
2006

3. Precipitation response to El Niño SST anomalies in the twentieth century

We first discuss the effect of increasing β in the 20C runs. As the impact of increasing the amplitude of $SSTA_{EN}$ is described in detail in Chung et al. (2013), we focus only on the $\alpha = 3$ case and use that as our control run: 20C ($\beta = 0$). In Fig. 4, the colored shading shows the 15-yr November–April-averaged precipitation in the equatorial Pacific (25°S–15°N, 120°E–60°W) for $0 \le \beta \le 1.3$. In each panel, the thick black lines show the location of the local meridional SST maxima ($SSTMAX_{mer}$), the red lines show the location of local precipitation maxima, and the arrows indicate the direction and magnitude of the surface winds. Local SST and precipitation maxima are identified as points at which the SST/precipitation values are larger than the values in neighboring grid points (measured north to south). The top panel ($\beta = 0$) corresponds to the 20C ($\beta = 0$) control run, in which only $SSTA_{3EN}$ is added. The panels below this correspond to the 20C ($0.3 \le \beta \le 1.3$) runs in which the residual $SSTA_R$ is added in multiples of $\beta = 0.3$, 0.6, 1.0, and 1.3.

The top panel ($\beta = 0$) shows the position of the SPCZ and ITCZ under 3 times the composite EN SST anomaly. Several differences between this and the observed CT EN precipitation pattern (Fig. 1) are noted. First, although the SPCZ is more zonal compared to its climatological position, it maintains a strong diagonal component and is distinctly separated from the ITCZ. Second, there is too much rainfall in the central equatorial Pacific, where the ITCZ and SPCZ merge. Moving down the panels, as β is gradually increased, the precipitation pattern resembles the observations more closely. The SPCZ becomes more zonal and the ITCZ spreads meridionally, forming a single band spanning the equatorial Pacific. The rainfall in the central Pacific, which is too high in the $\beta = 0$ case, decreases and becomes more realistic as β increases. The changes in the western Pacific and along the equator relative to $\beta = 0$ increase as β increases. These changes are statistically significant at the 95% level; see appendix A for a brief discussion on the method used to calculate significance and Fig A1 for maps showing areas of statistically significant precipitation change.

TABLE 2. Summary of ACCESS experiments described in this paper. From left to right, the columns show (i) the names of the runs, (ii) the multiplication factor β applied to the SST residual $SSTA_R$ (CT minus composite EN anomalies) added to the climatological SSTs, (iii) whether the CMIP3 MMEM GW pattern was added to the SSTs, (iv) the composite EN SST anomaly pattern multiplier, and (v) which background CO_2 level was used.

Name	β ($\times SSTA_R$)	Added ΔSST_{GW}	α ($\times SSTA_{EN}$)	CO_2 levels
20C_B0	0	No	3	346 ppm
20C_B1	0.3	No	3	346 ppm
20C_B2	0.6	No	3	346 ppm
20C_B3	1.0	No	3	346 ppm
20C_B4	1.3	No	3	346 ppm
21C_B0	0	Yes	3	730 ppm
21C_B1	0.3	Yes	3	730 ppm
21C_B2	0.6	Yes	3	730 ppm
21C_B3	1.0	Yes	3	730 ppm
21C_B4	1.3	Yes	3	730 ppm

The precipitation response is closely tied to the changes in SST. Over the western Pacific, the maximum precipitation lies directly over the region of warmest SSTs. Over the eastern Pacific, $SSTMAX_{mer}$ branches into three parts for $\beta = 0$. As β is increased, the branches merge into one for $\beta > 0.6$. For all β, the ITCZ lies over the northernmost branch of $SSTMAX_{mer}$, whereas for $\beta = 0$, the SPCZ lies to the south of the southernmost branch of $SSTMAX_{mer}$. To further clarify the relationship between rainfall and the SST pattern, the full SST field is shown in Fig. 5. As in Fig. 4, the red lines denote the local precipitation maxima (measured north–south), but the black lines now show the maximum zonal SST in the mapped region $SSTMAX_{zon}$. The meridional SST gradients, calculated as the off-equatorial SST mean (10°–5°S, 155°E–120°W) minus the equatorial SST mean (5°S–0°, 155°E–120°W) (Cai et al. 2012), are shown in the panels. For $\beta = 0$, it is clear that although the position of the ITCZ is influenced directly by the meridional $SSTMAX_{mer}$, the position of the SPCZ lies over the $SSTMAX_{zon}$ instead. As β is increased, $SSTMAX_{zon}$ shifts eastward from ~125°E ($\beta = 0$) to ~150°E ($\beta = 1.0$) at the equator.

The meridional SST gradients increase from −0.155 ($\beta = 0$) to 0.201 ($\beta = 1.3$). This is in apparent contrast to the findings of Cai et al. (2012), whose analysis of CMIP3 and CMIP5 models led to the conclusion that szCZ (zonal SPCZ) events occur during years when the meridional gradient is smallest. The gradients for $0 \le \beta \le 1.3$, canonical El Niño/La Niña, and climatological SSTs are shown in Fig. B1. The reason for this is that in our runs, the $3 \times \alpha$ EN SST anomaly added to climatological SSTs

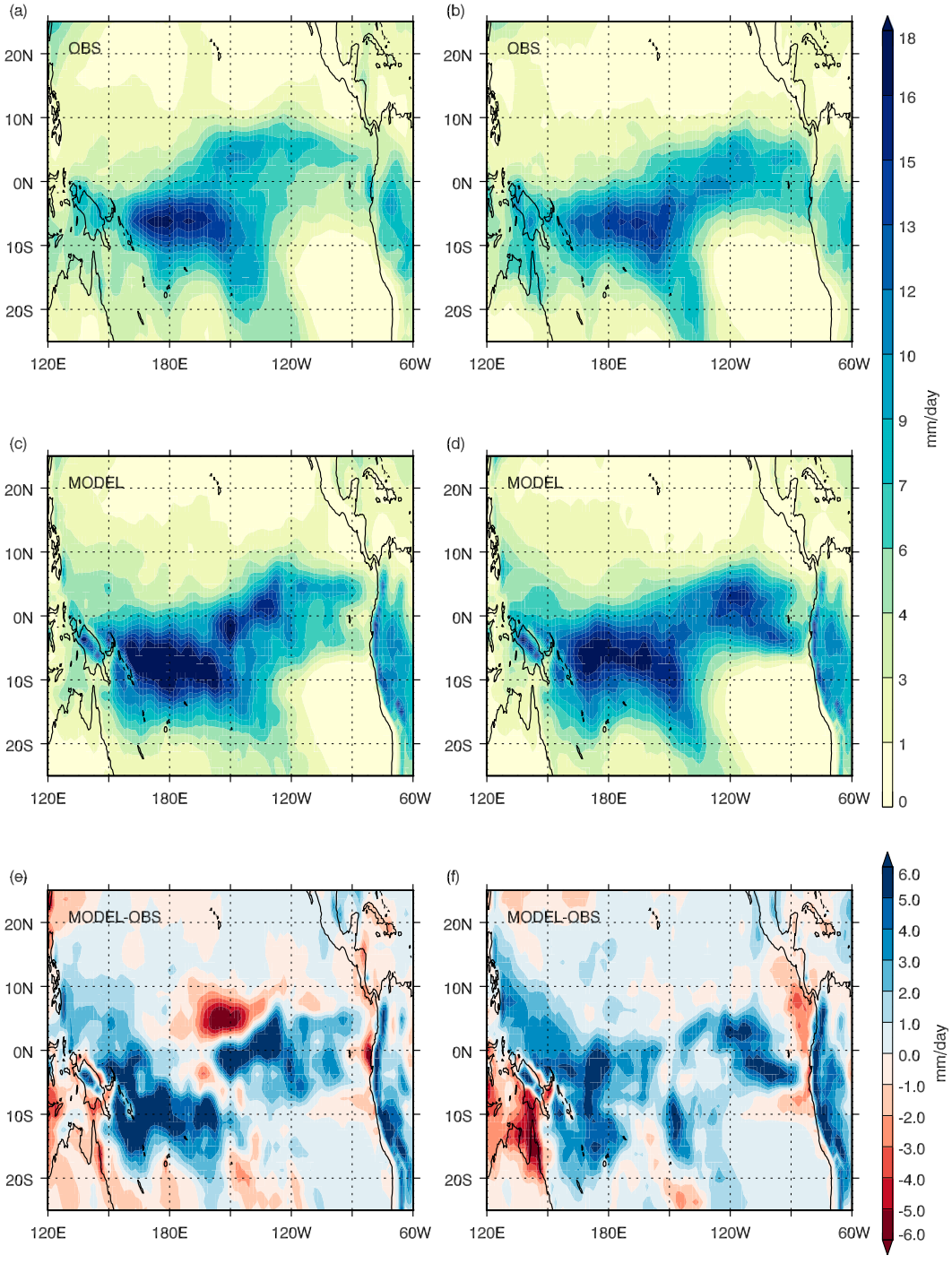

FIG. 3. (top) Observed November–April mean precipitation (CMAP) for (a) 1982/83 and (b) 1997/98. (middle) The precipitation response from the AGCM forced with observed, time-varying SSTs for (c) 1982/83 and (d) 1997/98. (bottom) The difference between the model response and CMAP observations for (e) 1982/83 and (f) 1997/98.

in the $\beta = 0$ case is artificially large and results in an SST pattern with extremely large warming over the equator. However, this illustrates the point that the meridional gradient alone is not a sufficient predictor of szCZ events. In addition to the gradient, the SST pattern and in particular both meridional and zonal SST maxima directly influence the precipitation patterns.

The change in precipitation δP is decomposed into dynamic δMCD, thermodynamic δTH, evaporative δE, and covariant δCOV terms using a simplified version of

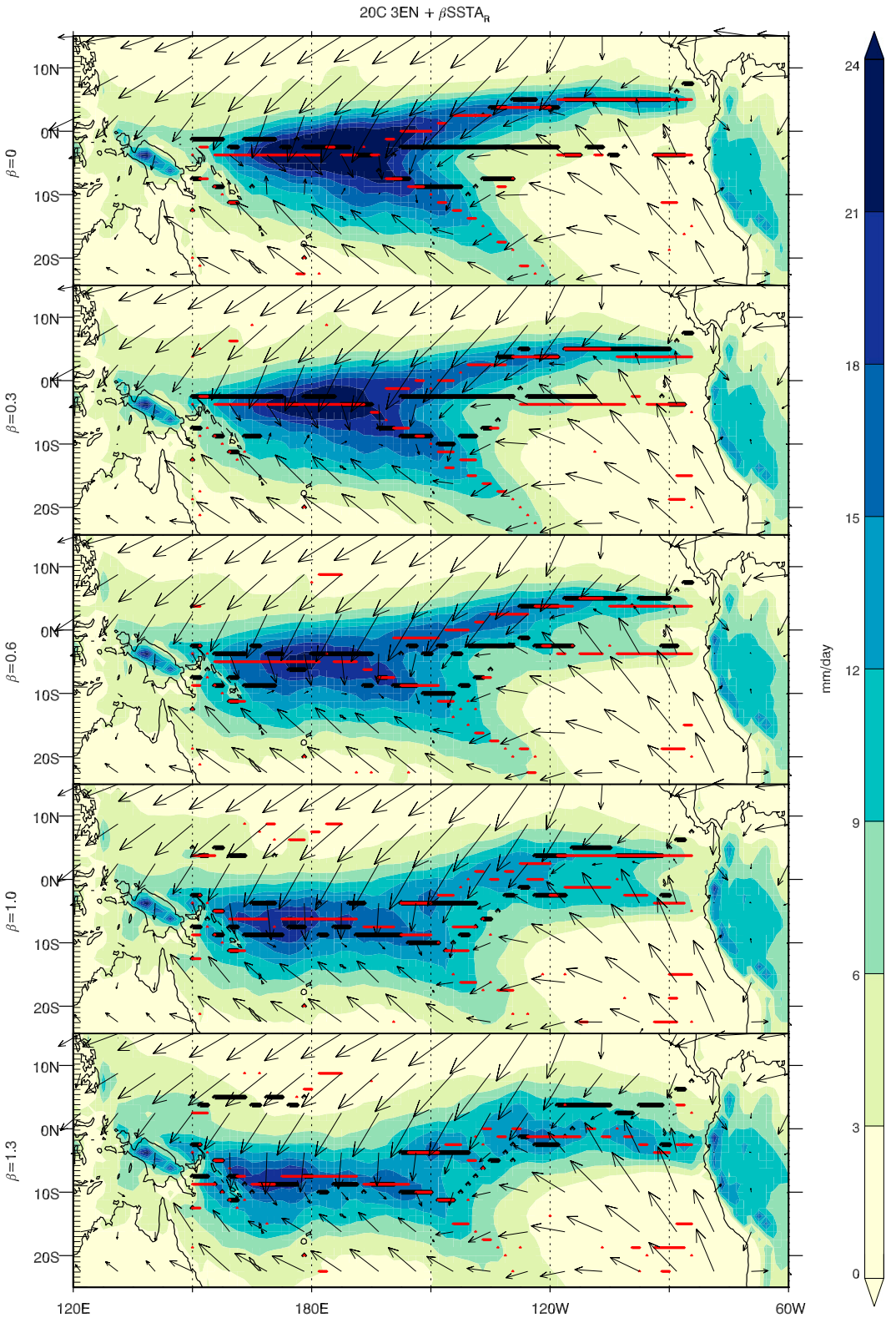

FIG. 4. Average 20C November–April precipitation from 15-yr model integrations using annually repeating 20C SST (climatological + 3EN SST anomalies) and CO_2 values (346 ppm). (top)–(bottom) $\beta = 0$, $\beta = 0.3$, $\beta = 0.6$, $\beta = 1.0$, and $\beta = 1.3$, where β is the strong EN residual pattern multiplier. The thick black lines indicate locations of local SST maxima, red lines show local precipitation maxima (both measured north–south), and the arrows indicate surface winds.

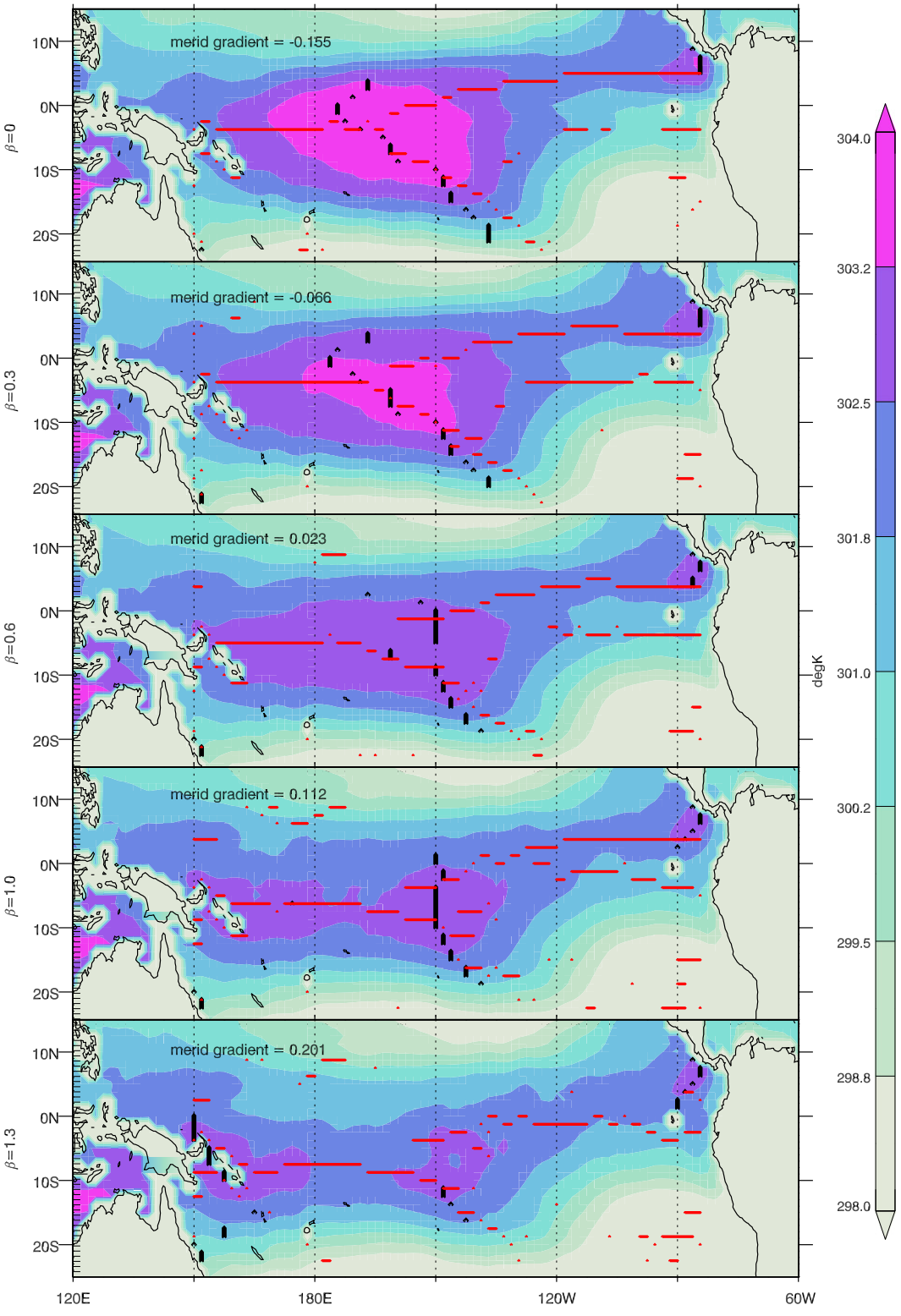

FIG. 5. Average 20C November–April SSTs used in model runs (climatological + 3EN SST anomalies). (top)–(bottom) $\beta = 0$, $\beta = 0.3$, $\beta = 0.6$, $\beta = 1.0$, and $\beta = 1.3$, where β is the strong EN residual pattern multiplier. The thick black lines indicate locations of the total zonal SST maximum in the mapped region, and red lines show local precipitation maxima (measured north–south).

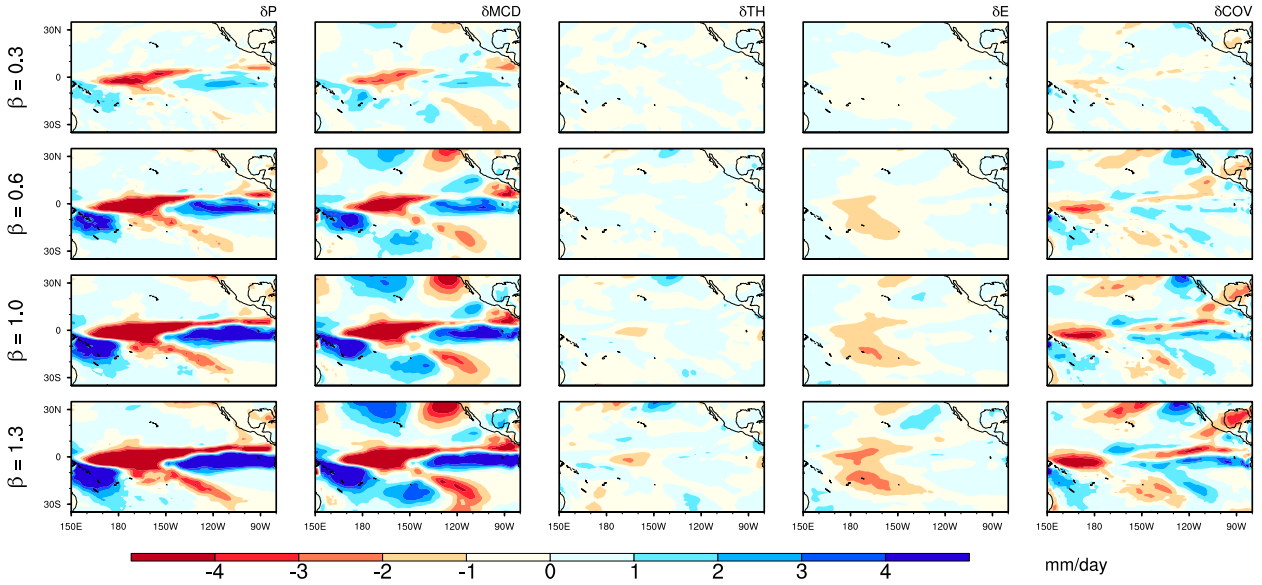

FIG. 6. In landscape mode, (left)–(right) 20C 15-yr average November–April precipitation anomalies (δP) and their dynamic δMCD, thermodynamic δTH, evaporative δE, and covariant δCOV contributions. (top)–(bottom) The rows correspond to changes between the control run ($\beta = 0$) and $\beta = 0.3$, $\beta = 0.6$, $\beta = 1.0$, and $\beta = 1.3$, where β is the CT EN residual pattern multiplier. Units are mm day^{-1}.

the Seager et al. (2010) method, detailed in Chung et al. (2013). The terms δTH and δMCD are defined to be

$$\delta\mathrm{TH} = -1/(\rho g)\int_0^{p_s} \nabla\cdot(\mathbf{u}_0[\delta q])\,dp \quad \text{and} \qquad (2)$$

$$\delta\mathrm{MCD} = -1/(\rho g)\int_0^{p_s} \nabla\cdot([\delta\mathbf{u}_0]q_0)\,dp, \qquad (3)$$

where ρ is the density of water, g is the acceleration due to gravity, p_s is the surface pressure, $\mathbf{u}$ is the horizontal wind vector, q is the specific humidity, and the subscript 0 denotes the values from the control run. The terms P, E, $\mathbf{u}$, and q are obtained from model output, whereas δCOV is defined to be the difference between δP and the sum of the other terms.

The terms are plotted over the Indo-Pacific region (35°S–35°N, 120°E–80°W) in Fig. 6. From left to right, the columns show δP, δMCD, δTH, δE, and δCOV. From top to bottom, the rows show the anomalies for $0.3 \le \beta \le 1.3$, calculated with respect to the $\beta = 0$ control run. The addition of SSTA_R introduces a dry anomaly in the central equatorial Pacific spanning ~170°E–150°W, bounded to the east and west by wet anomalies. There is also a drying along the eastern part of the SPCZ (which gives rise to its zonal orientation) and the northeastern part of the ITCZ. The dynamic component δMCD is the main contributor to δP, with smaller contributions from δCOV and δE. Note that along the SPCZ, the contributions from δCOV and δE counteract the contribution from δMCD.

a. *Nonlinear response to increasing* SSTA_R

Nonlinearities in the precipitation response are defined to be the difference between the $\beta \ge 0.6$ response and what the changes would be if the $\beta = 0.3$ response was multiplied linearly, for example,

$$\delta P(\mathrm{NL})_{\beta=0.6} = \delta P_{\beta=0.6} - (2 \times \delta P_{\beta=0.3}). \qquad (4)$$

We find that the nonlinearities in precipitation response for $0.6 \le \beta \le 1.3$ are noisy, and although their amplitude increases with β, they are not statistically significant.

b. *Precipitation response to increasing* SSTA_R *in the absence of* $\mathrm{SSTA}_{3\mathrm{EN}}$

To determine the effect of adding only SSTA_R, without $\mathrm{SSTA}_{3\mathrm{EN}}$, we repeated the 20C runs adding only $\beta \times \mathrm{SSTA}_R$ to the climatological SSTs. The results are shown in Fig. 7, where the rows correspond to $\beta = 0, 0.3, 0.6, 1.0$, and 1.3 from top to bottom. As β increases, two key changes occur: (i) the ITCZ dries, and (ii) the southeastern tip of the SPCZ retreats northwestward and the maximum rainfall in the SPCZ shifts southward. The movement of the precipitation bands follows the branches of $\mathrm{SSTMAX}_{\mathrm{mer}}$, which move farther apart instead of merging.

While gradually increasing the amplitude of SSTA_R in the absence of $\mathrm{SSTA}_{3\mathrm{EN}}$ does significantly change the precipitation patterns, it does not result in a szCZ event. It is therefore necessary to have both the large-amplitude SST anomaly provided by $\mathrm{SSTA}_{3\mathrm{EN}}$ as well as the detailed spatial variations from SSTA_R to generate a szCZ.

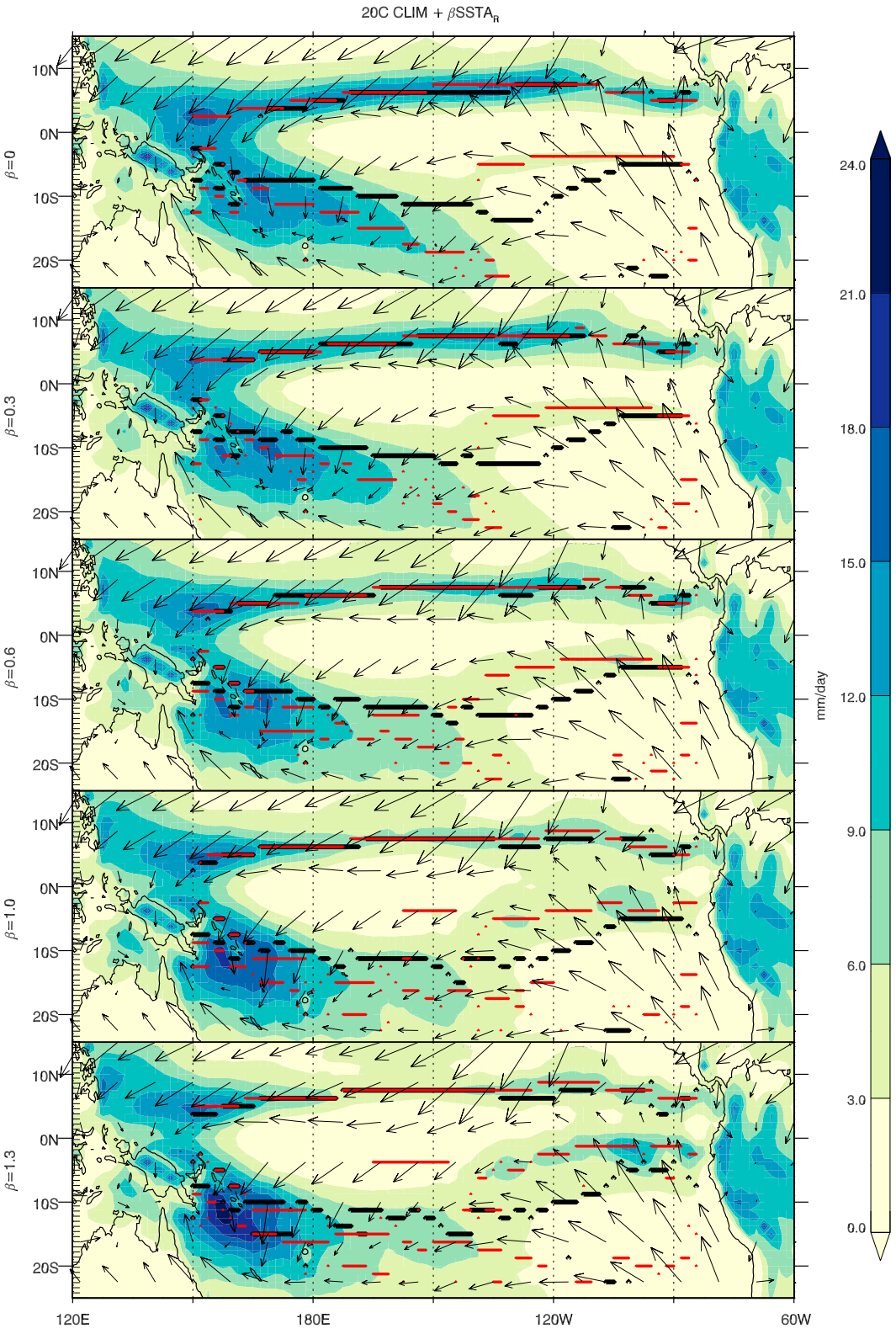

FIG. 7. Average 20C November–April precipitation from 15-yr model integrations using annually repeating 20C climatological SSTs (without added EN SST anomalies) and CO_2 values (346 ppm): (top)–(bottom) $\beta = 0$, $\beta = 0.3$, $\beta = 0.6$, $\beta = 1.0$, and $\beta = 1.3$, where β is the strong EN residual pattern multiplier $SSTA_R$ (Fig. 2c). The thick black lines indicate locations of local SST maxima, red lines show local precipitation maxima, and the arrows indicate surface winds. Units are mm day^{-1}.

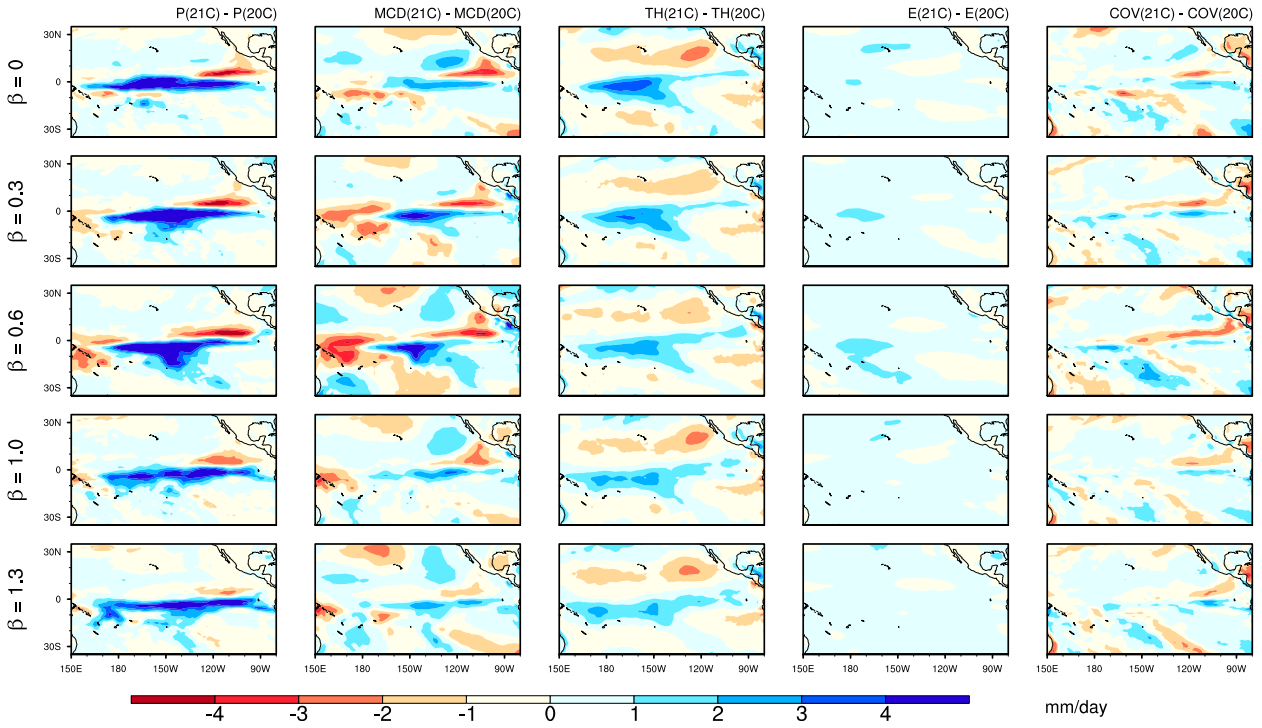

FIG. 8. Differences between the 20C and 21C runs, where the global warming SST pattern ΔSST_{GW} is added and the CO_2 level is increased to 730 ppm. In landscape mode, (left)–(right) the 15-yr average November–April changes in total precipitation P, and its breakdown into dynamic MCD, thermodynamic TH, evaporative E, and covariant COV terms. (top)–(bottom) The rows correspond to $\beta = 0$, $\beta = 0.3$, $\beta = 0.6$, $\beta = 1.0$, and $\beta = 1.3$, where β is the CT residual pattern multiplier. Units are mm day^{-1}.

4. Impact of global warming

To simulate the 21C climate, we repeated the runs, adding a global warming SST pattern ΔSST_{GW} to the SSTs used in the 20C runs. We therefore applied the sum of the climatological SSTs, $SSTA_{3EN}$, β $SSTA_R$, and ΔSST_{GW}. The CO_2 level was also increased to 730 ppm. Figure 8 shows, from left to right, the changes in P, MCD, TH, E, and COV for $0 \le \beta \le 1.3$, for example, $P_\beta(21C) - P_\beta(20C)$. The addition of ΔSST_{GW} increases the precipitation along the equator for all values of β. It also dries the northeastern part of the ITCZ. However, as β increases, the maximum precipitation anomaly along the equator shifts eastward and weakens, and the amount of drying along the ITCZ decreases relative to the control ($\beta = 0$). The dynamic component contributes significantly to the precipitation anomalies; however, the thermodynamic and covariant terms are also comparable. The contribution from the thermodynamic term, which increases rainfall in the western equatorial Pacific, decreases as β increases.

While Fig. 8 shows how precipitation changes, case by case, for $0 \le \beta \le 1.3$, it is also important to know how adding ΔSST_{GW} affects the $SSTA_R$-driven changes. In other words, as β increases, how do the precipitation anomalies with respect to the control run δP change under global warming? In Fig. 9, we plot the differences in anomalies between the 20C and 21C runs, with respect to the 20C control run. From left to right, the columns show the changes in precipitation anomalies, for example, $\delta P(21C) - \delta P(20C)$, and their dynamic, thermodynamic, evaporative, and covariant components. The rows correspond to $\beta = 0.3$, 0.6, 1.0, and 1.3.

One feature common for all values of β is the decrease in precipitation along the central equatorial Pacific. For $\beta \le 0.6$, this enhanced drying extends west to 150°E. To the south of this dry band, there is increased precipitation along the central Pacific, around approximately 5°–20°S, 160°E–120°W. This overlaps some of the dry anomalies seen in Fig. 8, indicating that in the 21C runs, this region does not dry as much as in the 20C runs. Therefore, the addition of ΔSST_{GW} affects the precipitation response to $SSTA_R$ differently in different regions: it enhances the $SSTA_R$-driven drying along the equatorial Pacific, but reduces it around the region 5°–20°S, 160°E–120°W. As with the 20C case, the changes in the precipitation anomalies are dominated by the atmospheric circulation dynamics.

Regions of interest

To highlight specific changes in the precipitation structure and amplitude due to increasing β, we plot the

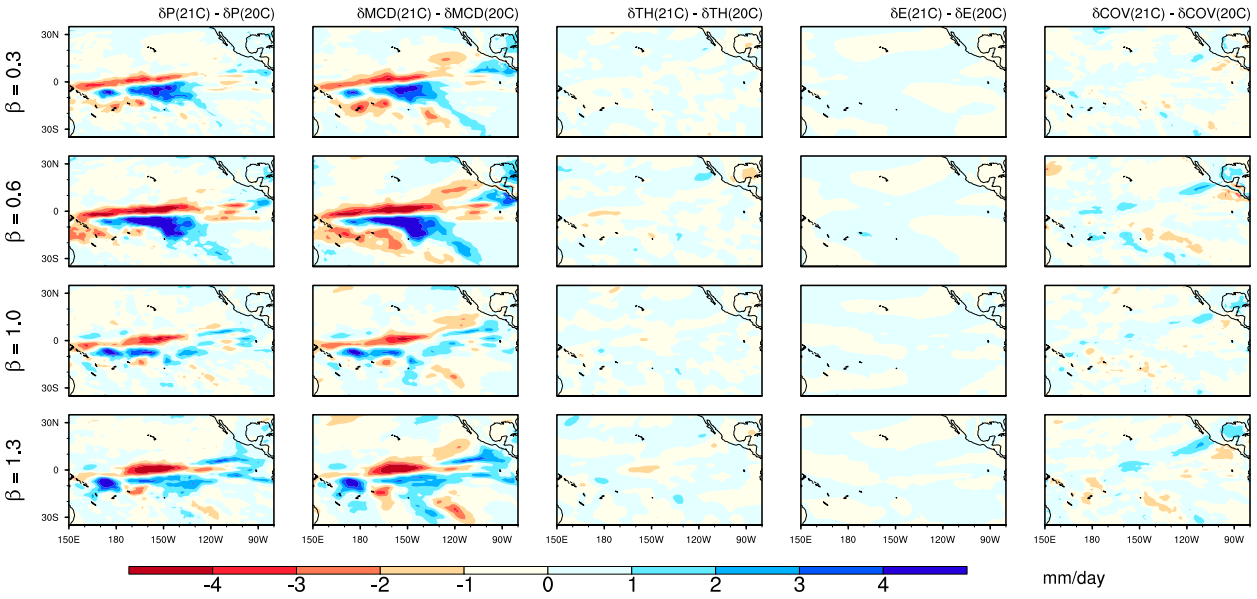

FIG. 9. In landscape mode, (left)–(right) the 15-yr average November–April changes in EN residual ($SSTA_R$)-driven anomalies in precipitation δP, and its dynamic δMCD, thermodynamic δTH, evaporative δE, and covariant δCOV terms between the 20C and 21C runs, for example, δP(21C)–δP(20C). (top)–(bottom) The rows correspond to $\beta = 0.3$, $\beta = 0.6$, $\beta = 1.0$, and $\beta = 1.3$, where β is the CT EN residual pattern multiplier. Units are mm day^{-1}.

precipitation profiles along certain lines of latitude and longitude in Fig. 10. Figures 10a, 10b, and 10c show the profiles along the equator, 20°S, and 219.4°E, respectively. Each colored line corresponds to a value of β, solid lines denote the 20C runs, and dotted lines denote the 21C runs. The area between the 20C and 21C profiles is stippled to emphasize how the precipitation changes in each run. Each panel highlights a different feature of the changes. Note that in Fig. 10, the $\beta = 0$ case is *not* the climatology but has 3 times the composite EN SST anomaly added. We therefore demonstrate the shortcomings of simply multiplying the amplitude of the SST anomaly and how adding structural details is important in reproducing the observed precipitation response. GPCP and CMAP observations for the two szCZ events, averaged, are plotted with orange and pink lines, respectively.

First, Fig. 10a shows how the maximum precipitation anomaly along the equator shifts eastward as β increases. The shift is apparent in both 20C and 21C runs, although there is generally more precipitation in the 21C runs. One exception is that for $\beta \leq 0.6$; the precipitation to the west of the maximum anomaly decreases in the 21C runs. Comparing the 20C ($\beta = 1$) case (blue) with the observations, the shape of the profile matches well, although the overall amount of precipitation is overestimated. For $\beta = 1.3$ (not shown), the maximum precipitation anomaly is too far east compared to observations.

The second feature, shown in Fig. 10b, is the increasing zonality of the SPCZ. This is illustrated using the rainfall profile along 20°S. In the $\beta = 0$ case, where the SPCZ has a diagonal component, only the southeast tip crosses 20°S. As β increases, the northwest part of the SPCZ shifts southward, while the southeast tip retreats northwestward. This results in increased rainfall in the west and decreased rainfall in the east. Along 20°S, the changes between the 20C and 21C runs are relatively small and highly dependent on both the longitude and value of β.

Last, Fig. 10c shows the rainfall profile along 219.4°E longitude and highlights the meridional spreading and southward shift of the ITCZ and the merging of the SPCZ and ITCZ into a single precipitation band. Note that in the $\beta = 0$ case (black lines), the SPCZ and ITCZ are clearly distinguishable. Additionally, the precipitation along the equator is overestimated by a factor of ~2. As β increases, the two peaks in the precipitation profile decrease in amplitude and merge. Overall, the 21C runs produce significantly greater precipitation to the south of the ITCZ peak and slightly less to the north of the peak. In the 21C runs, the ITCZ is also shifted southward, resulting in a more efficient merging of the ITCZ and SPCZ. The $\beta = 1.0$ case agrees reasonably well with the observations, although it is not a perfect match. In the 20C $\beta = 1.0$ run (blue solid line), the model produces too much precipitation in the south, resulting in a second precipitation maximum around 17°S. Interestingly, the 21C $\beta = 1.0$ run (blue dashed line) produces a precipitation profile that more closely resembles the GPCP

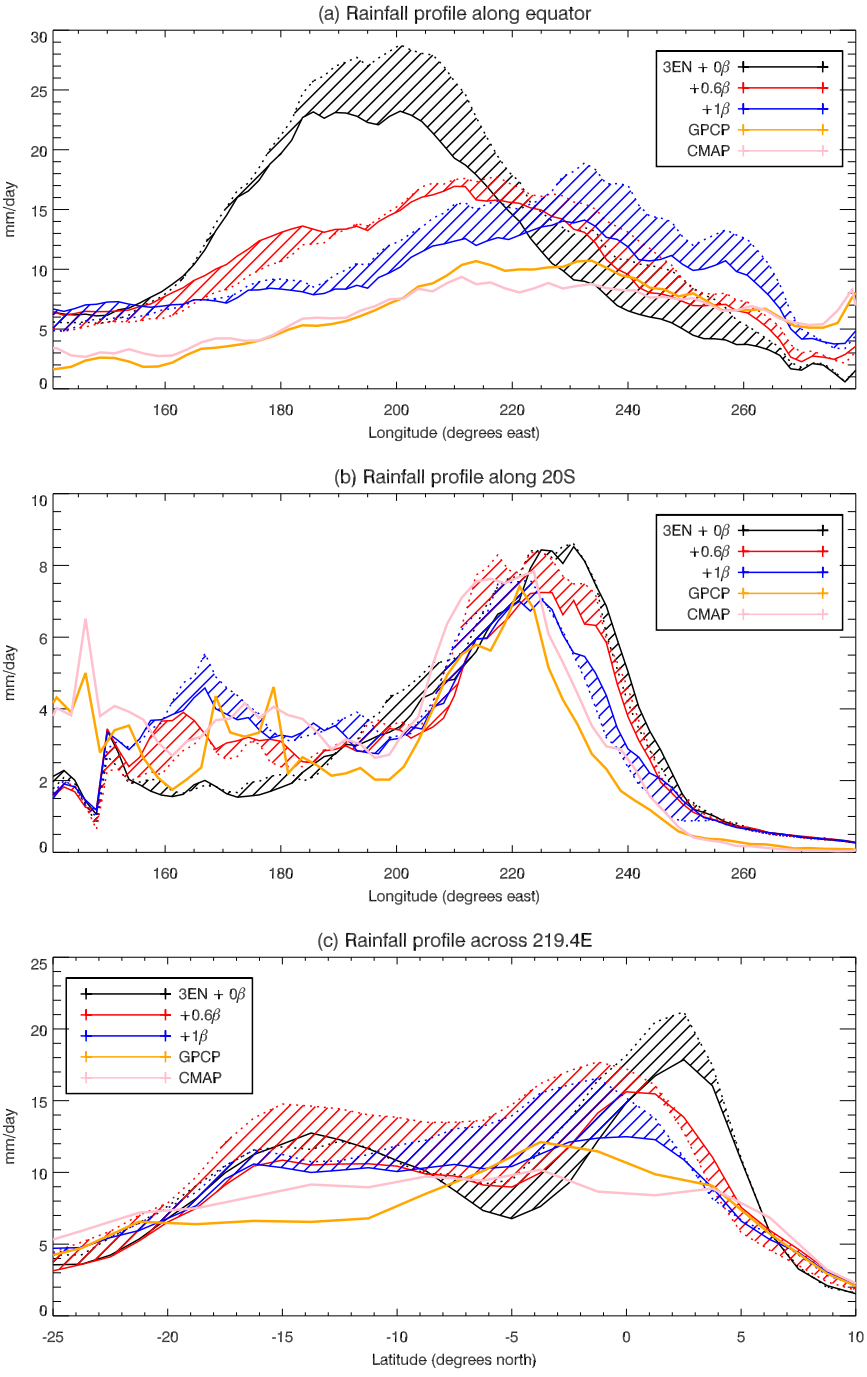

FIG. 10. Rainfall profiles along (a) the equator, (b) 20°S, and (c) 219.4°E. Thick solid lines represent the 20C runs, and dotted lines represent the 21C runs. The areas between the 21C and 20C runs are stippled to highlight the precipitation changes. Orange and pink lines show GPCP and CMAP observations (for 1982/83 and 1997/98, averaged) respectively.

profile, although there is more precipitation overall. Note, however, that there is some discrepancy between the GPCP and CMAP observations in this region.

Figure 11 shows the (Fig. 11a) spatial correlation and (Fig. 11b) root-mean-square error (RMSE) between the precipitation in each of the 20C runs and the following: (i) the $\beta = 1$ run (solid line) and (ii) GPCP and (iii) CMAP observations of the CT EN events (dotted and dashed lines, respectively). The datasets are correlated in the tropical Pacific (25°S–25°N, 150°–280°E). This figure

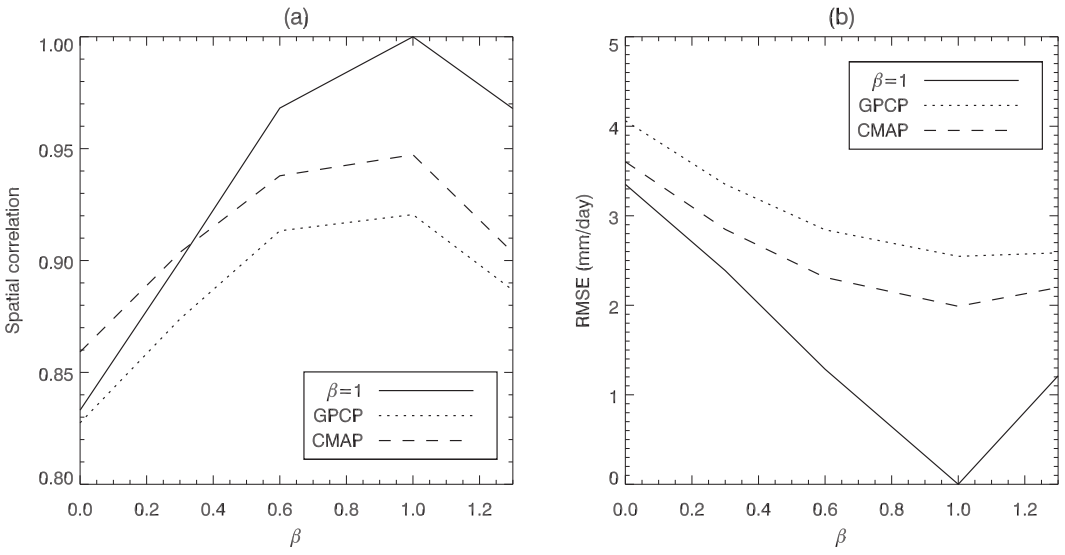

FIG. 11. (a) Spatial correlation and (b) root-mean-square error of precipitation between the 20C runs ($0 \leq \beta \leq 1.3$) and $\beta = 1$ (solid line), as well as observations of CT EN events from GPCP (dotted lines) and CMAP (dashed lines) datasets. The region considered is the tropical Pacific (25°S–25°N, 150°–280°E).

reiterates the importance of $SSTA_R$ as the correlation between the 20C runs and observations peaks, and the RMSE is minimized for $\beta = 1$. The model therefore most accurately reproduces the szCZ precipitation pattern when the full $SSTA_R$ is applied.

5. Discussion and summary

We investigated the SSTAs that caused the distinctive precipitation patterns that occurred during the years 1982/83 and 1997/98, when the ITCZ and SPCZ merged into a single zonal convergence zone (szCZ) stretching across the South Pacific at ~5°S. To determine the relative importance of the SST structure and the magnitude of its anomalies, we investigated the effects of varying the spatial structure of an El Niño SST anomaly on the precipitation response in the Indo-Pacific region. We calculated a residual SST anomaly $SSTA_R$: the difference between the average SST anomaly from CT El Niño events and a large-amplitude composite El Niño SST anomaly $SSTA_{3EN}$. When our atmospheric general circulation model (AGCM) is forced with just $SSTA_{3EN}$ added to the climatological SSTs, the SPCZ becomes slightly more zonal but does not merge fully with the ITCZ. The amount of precipitation along the equator is also overestimated. Likewise, when the AGCM is forced with just $SSTA_R$ added to climatological SSTs, the precipitation patterns change, but a szCZ is not generated. The addition of both $SSTA_R$ and $SSTA_{3EN}$ is therefore crucial in obtaining the correct amplitude and structure of the precipitation response.

Various aspects of the SST field and its relationship to the precipitation pattern were investigated, including the meridional SST gradient, the local meridional SST maxima ($SSTMAX_{mer}$), and the zonal SST maximum ($SSTMAX_{zon}$). We found that for all values of β, the maximum rainfall over the western Pacific and ITCZ lie directly over $SSTMAX_{mer}$. The position of the SPCZ, however, is more closely linked to $SSTMAX_{zon}$. As β is increased, both the maximum equatorial precipitation and $SSTMAX_{zon}$ shift east. Although Cai et al. (2012) found that szCZ (or zonal SPCZ) events occur when the meridional gradient decreases compared to other years, we found that the meridional gradient *increases* as β is increased. This is because the applied $SSTA_{3EN}$ SST pattern produces an extremely warm central equatorial Pacific region, which cools as β increases. The $\beta = 0$ case is idealized and therefore not in a part of parameter space considered by Cai et al. (2012). Therefore, in the case of these extreme SST patterns, the meridional SST gradient itself is not a sufficient predictor of szCZ events.

A simplified breakdown of the moisture budget shows that the precipitation changes due to increasing $SSTA_R$ are dominated by changes in the atmospheric circulation. While Chung et al. (2013) found several major nonlinearities in the precipitation response to a linear increase in the amplitude of $SSTA_{EN}$, we found no statistically significant nonlinearities when increasing the amplitude of $SSTA_R$ only.

To test how the response would change in the twenty-first century under global warming, the CMIP3 A2 MMEM global warming SST pattern (2080–99 − 1980–99) ΔSST_{GW} was added to the SST anomalies. Additionally, the CO_2 concentration was increased from 346 to 730 ppm. Global warming increases the precipitation along the

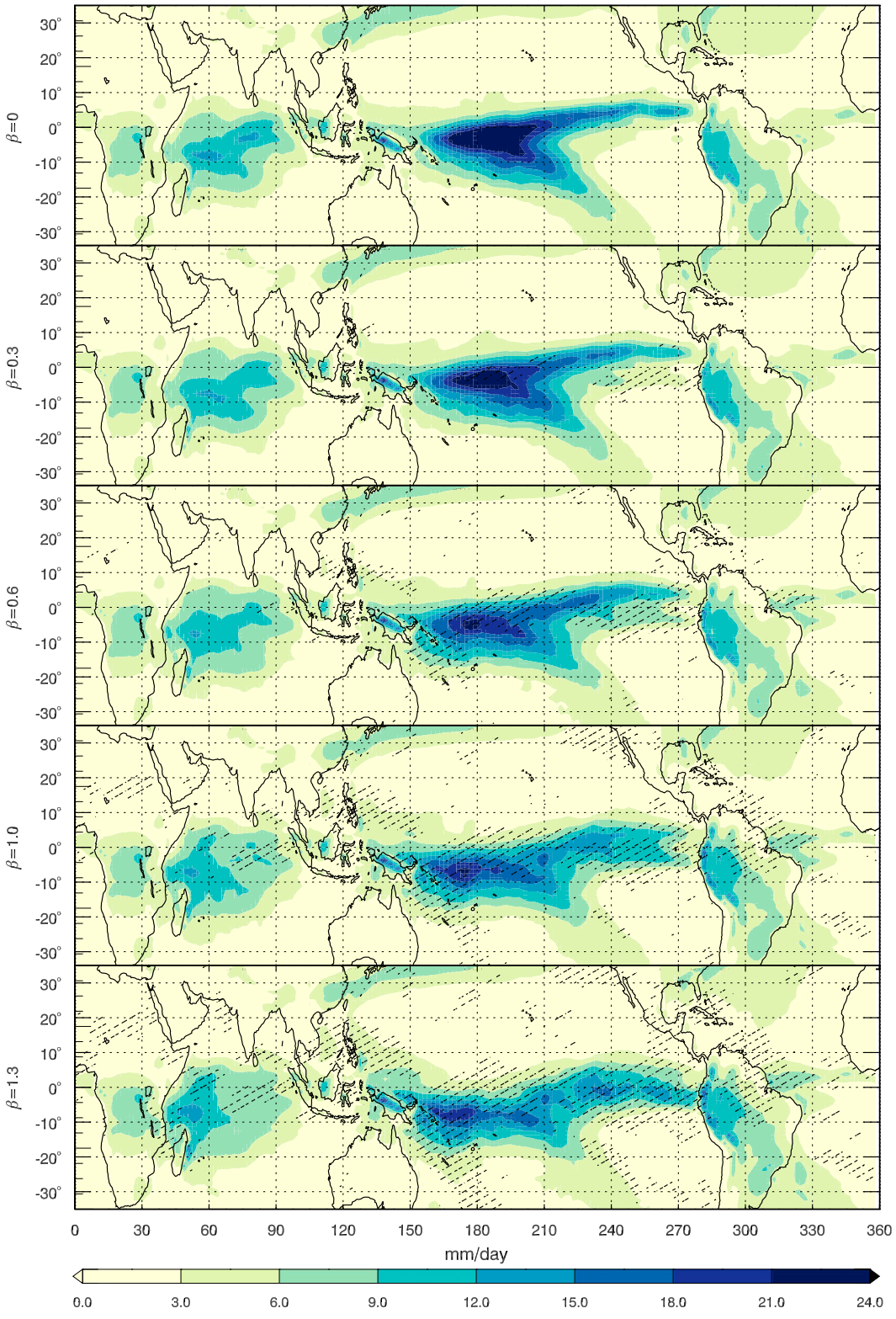

FIG. A1. As in Fig. 4, but highlighting statistically significant changes. Average 20C November–April precipitation from 15-yr model integrations using annually repeating 20C SST and CO2 values (346 ppm): (top)–(bottom) $\beta = 0$, $\beta = 0.3$, $\beta = 0.6$, $\beta = 1.0$, and $\beta = 1.3$, where β is the CT EN residual pattern multiplier. Stippling indicates areas where the precipitation changes relative to $\beta = 0$ are statistically significant at the 95% level.

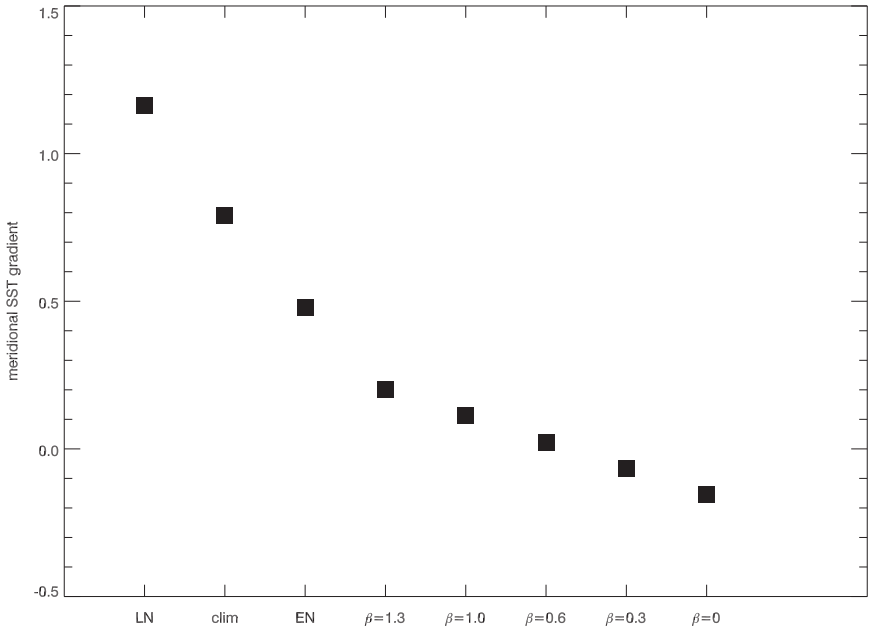

FIG. B1. Meridional SST gradients for canonical La Niña and El Niño SSTs (the average of all events between 1979 and 2009), 1979–2009 climatological SSTs, and SSTs from the 20C runs ($0 \le \beta \le 1.3$).

equator and decreases precipitation over the northeastern part of the ITCZ, shifting the ITCZ equatorward. This enhances the rainfall increase caused by $SSTA_R$ in the western equatorial Pacific but counteracts the drying caused by $SSTA_R$ in the central equatorial Pacific.

Our results are consistent with projections from the SRES A2 scenario from the CMIP3 models that project a precipitation increase in the ITCZ in the twenty-first century (Australian Bureau of Meteorology and CSIRO 2011a,b). However, we note that these experiments do not provide a quantitative measure on the relative change in frequency of zonal SPCZ events under global warming. They suggest that the response to large-amplitude EN events is enhanced, along with the response to $SSTA_R$ in the eastern and western Pacific. Several key caveats to our work should also be noted: (i) the results presented here are subject to model bias; (ii) although most models agree that SSTs will warm most along the equator, the variations in the detailed structure of the ΔSST_{GW} pattern can affect the precipitation response significantly; and (iii) there is also uncertainty regarding how EN events will change in the twenty-first century (e.g., Collins et al. 2010). We also note that while we have shown that both $SSTA_R$ and $SSTA_{3EN}$ are necessary to generate a szCZ, it is theoretically possible for another, yet unobserved, SST pattern to do so.

In summary, we find that in order to generate a szCZ precipitation pattern, both large-amplitude El Niño SST anomalies and the SST residual observed during szCZ years are necessary. It is the differences in the SSTA patterns between the canonical EN SSTs and the SSTs observed during 1982/83 and 1997/98 that are crucial to the generation of szCZ events. We identify three key factors that influence the precipitation patterns: (i) The local meridional SST maxima influence the position of the ITCZ and western Pacific rainfall maxima. (ii) The zonal SST maximum influences the position of the SPCZ. (iii) The total SST influences the amount of precipitation over the western and central equatorial Pacific. Additionally, in some extreme cases, such as in some of our experiments, a decreasing meridional SST gradient may not be a sufficient predictor of a szCZ event. Under global warming, precipitation increases in most locations along the equatorial Pacific, and some effects of the SST residual are enhanced, such as the southward shift of the ITCZ. From these experiments alone it is not possible to determine whether the frequency of szCZ events will change under global warming. However, we can conclude that for a given value of β, a more zonal precipitation pattern is generated under global warming.

Acknowledgments. This work was supported by the Pacific–Australia Climate Change Science and Adaptation Planning Program (PACCSAP), a program supported by AusAID, in collaboration with the Department of Climate Change and Energy Efficiency, and delivered by the Bureau of Meteorology and the Commonwealth Scientific

and Industrial Research Organisation (CSIRO). Support for this work was also provided by the Australian Climate Change Science Program (ACCSP). We thank Brad Murphy, Ian Smith, and anonymous reviewers for extremely helpful comments on the manuscript. We acknowledge the modeling groups, the Program for Climate Model Diagnosis and Intercomparison (PCMDI), and the WCRP's Working Group on Coupled Modelling (WGCM) for their roles in making available the WCRP CMIP3 multimodel dataset. Support of this dataset is provided by the Office of Science, U.S. Department of Energy.

APPENDIX A

Calculation of Statistical Significance

To calculate the statistical significance of the precipitation response at each grid point, we pool the data from each comparison run: 20C ($0.3 \le \beta \le 1.3$) with the data from the control run 20C ($\beta = 0$). At each grid point, the data from each integration year is sorted, ranked, and the median calculated. Assuming a binomial distribution, a change that is ≥95% significant would require ≥12 (of 15) data points from the comparison run to be greater or larger than the median. Figure A1 shows the precipitation response in the 20C runs, shown in Fig. 4, with areas that have statistically significant changes stippled.

APPENDIX B

Meridional SST Gradients

The meridional SST gradients are defined to be the off-equatorial SST mean (10°–5°S, 155°E–120°W) minus the equatorial SST mean (5°S–0°, 155°E–120°W) (Cai et al. 2012). We calculate this for $0 \le \beta \le 1.3$ and also for three other cases: a canonical La Niña SST pattern, climatological SSTs, and a canonical El Niño SST pattern. The gradients are plotted in Fig. B1, showing that a decrease in meridional SST gradient does not necessarily result in a szCZ event (as in the case of $\beta < 1$).

REFERENCES

Adler, R. F., and Coauthors, 2003: The version-2 Global Precipitation Climatology Project (GPCP) monthly precipitation analysis (1979–present). *J. Hydrometeor.,* **4,** 1147–1167, doi:10.1175/1525-7541(2003)004<1147:TVGPCP>2.0.CO;2.

Australian Bureau of Meteorology and CSIRO, 2011a: *Regional Overview.* Vol. 1, *Climate Change in the Pacific: Scientific Assessment and New Research,* Australian Bureau of Meteorology, 257 pp. [Available online at www.pacificclimatechangescience.org/publications/reports/report-climate-change-in-the-pacific-scientific-assessment-and-new-research.]

——, 2011b: *Country Reports.* Vol. 2, *Climate Change in the Pacific: Scientific Assessment and New Research,* Australian Bureau of Meteorology, 273 pp. [Available online at www.pacificclimatechangescience.org/publications/reports/report-climate-change-in-the-pacific-scientific-assessment-and-new-research.]

Bi, D., and Coauthors, 2012: The ACCESS coupled model: Description, control climate and preliminary validation. *Aust. Meteor. Ocean J.,* **63,** 41–64.

Brown, J. R., S. B. Power, F. P. Delage, R. A. Colman, A. F. Moise, and B. F. Murphy, 2011: Evaluation of the South Pacific convergence zone in IPCC AR4 climate model simulations of the twentieth century. *J. Climate,* **24,** 1565–1582, doi:10.1175/2010JCLI3942.1.

Cai, W., and Coauthors, 2012: More extreme swings of the South Pacific convergence zone due to greenhouse warming. *Nature,* **488,** 365–369, doi:10.1038/nature11358.

——, and Coauthors, 2014: Increasing frequency of extreme El Niño events due to greenhouse warming. *Nat. Climate Change,* **4,** 111–116, doi:10.1038/nclimate2100.

Chung, C., S. B. Power, J. Arblaster, H. Rashid, and G. Roff, 2013: Nonlinear precipitation response to El Niño and global warming in the Indo-Pacific. *Climate Dyn.,* **42,** 1837–1856, doi:10.1007/s00382-013-1892-8.

Collins, M., and Coauthors, 2010: The impact of global warming on the tropical Pacific Ocean and El Niño. *Nat. Geosci.,* **3,** 391–397, doi:10.1038/ngeo868.

Davies, T., M. J. P. Cullen, A. J. Malcolm, M. H. Mawson, A. Staniforth, A. A. White, and N. Wood, 2005: A new dynamical core for the Met Office's global and regional modelling of the atmosphere. *Quart. J. Roy. Meteor. Soc.,* **131,** 1759–1782, doi:10.1256/qj.04.101.

Huffman, G. J., R. F. Adler, D. T. Bolvin, and G. Gu, 2009: Improving the global precipitation record: GPCP version 2.1. *Geophys. Res. Lett.,* **36,** L17808, doi:10.1029/2009GL040000.

Hurrell, J. W., J. J. Hack, D. Shea, J. M. Caron, and J. Rosinski, 2008: A new sea surface temperature and sea ice boundary dataset for the Community Atmosphere Model. *J. Climate,* **21,** 5145–5153, doi:10.1175/2008JCLI2292.1.

Kim, W., and W. Cai, 2013: Second peak in the far eastern Pacific sea surface temperature anomaly following strong El Niño events. *Geophys. Res. Lett.,* **40,** 4751–4755, doi:10.1002/grl.50697.

Kug, J.-S., F.-F. Jin, and S.-I. An, 2009: Two types of El Niño events: Cold tongue El Niño and warm pool El Niño. *J. Climate,* **22,** 1499–1515, doi:10.1175/2008JCLI2624.1.

Lengaigne, M., and G. A. Vecchi, 2009: Contrasting the termination of moderate and extreme El Niño events in coupled general circulation models. *Climate Dyn.,* **35,** 299–313, doi:10.1007/s00382-009-0562-3.

Martin, G. M., S. F. Milton, C. A. Senior, M. E. Brooks, S. Ineson, T. Reichler, and J. Kim, 2010: Analysis and reduction of systematic errors through a seamless approach to modeling weather and climate. *J. Climate,* **23,** 5933–5957, doi:10.1175/2010JCLI3541.1.

——, and Coauthors, 2011: The HadGEM2 family of Met Office Unified Model climate configurations. *Geosci. Model Dev. Discuss.,* **4,** 765–841, doi:10.5194/gmdd-4-765-2011.

McPhaden, M., 1999: Genesis and evolution of the 1997-98 El Niño. *Science,* **283,** 950–954, doi:10.1126/science.283.5404.950.

——, S. Zebiak, and M. Glantz, 2006: ENSO as an integrating concept in earth science. *Science,* **314,** 1740–1745, doi:10.1126/science.1132588.

Meehl, G. A., and Coauthors, 2007: Global climate projections. *Climate Change 2007: The Physical Science Basis,* S. Solomon et al., Eds., Cambridge University Press, 747–845.

Murphy, B., S. Power, and S. McGree, 2014: The varied impacts of El Niño–Southern Oscillation on Pacific island climates. *J. Climate,* **27,** 4015–4036, doi:10.1175/JCLI-D-13-00130.1.

Philander, S., 1990: *El Niño, La Niña, and the Southern Oscillation.* Academic Press, 293 pp.

Power, S., M. Haylock, R. Colman, and X. Wang, 2006: The predictability of interdecadal changes in ENSO and ENSO teleconnections. *J. Climate,* **19,** 4755–4771, doi:10.1175/JCLI3868.1.

——, F. Delage, C. T. Y. Chung, G. Kociuba, and K. Keay, 2013: Robust twenty-first-century projections of El Niño and related precipitation variability. *Nature,* **502,** 541–547, doi:10.1038/nature12580.

Seager, R., N. Naik, and G. Vecchi, 2010: Thermodynamic and dynamic mechanisms for large-scale changes in the hydrological cycle in response to global warming. *J. Climate,* **23,** 4651–4668, doi:10.1175/2010JCLI3655.1.

Staniforth, A., A. White, and N. Wood, 2003: Analysis of semi-Lagrangian trajectory computations. *Quart. J. Roy. Meteor. Soc.,* **129,** 2065–2085, doi:10.1256/qj.02.115.

Takayabu, Y. N., T. Iguchi, K. Misako, A. Shibata, and H. Kanzawa, 1999: Abrupt termination of the 1997–98 El Niño in response to a Madden–Julian oscillation. *Nature,* **402,** 279–282, doi:10.1038/46254.

Vecchi, G. A., and D. E. Harrison, 2006: The termination of the 1997–98 El Niño. Part I: Mechanisms of oceanic change. *J. Climate,* **19,** 2633–2646, doi:10.1175/JCLI3776.1.

Vincent, E., M. Lengaigne, C. Menkes, N. Jourdain, P. Marchesiello, and G. Madec, 2011: Interannual variability of the South Pacific convergence zone and implications for tropical cyclone genesis. *Climate Dyn.,* **36,** 1881–1896, doi:10.1007/s00382-009-0716-3.

Widlansky, M. J., A. Timmermann, K. Stein, S. McGregor, N. Schneider, M. H. England, M. Lengaigne, and W. Cai, 2013: Changes in South Pacific rainfall bands in a warming climate. *Nat. Climate Change,* **3,** 417–423, doi:10.1038/nclimate1726.

Yeh, S., J. Kug, B. Dewitte, M. Kwon, B. Kirtman, and F. Jin, 2009: El Niño in a changing climate. *Nature,* **461,** 511–514, doi:10.1038/nature08316.